4G Signal Propagation at Ground Level

Peter J. Burke, *Fellow, IEEE*

***Abstract*— The primary purpose of this article is to demonstrate experimentally and explain theoretically (based on physics-based literature and empirical-based industry-standard models) that, in the limit where the receiver height vanishes above an imperfectly conducting plane such as the surface of the Earth, the propagation characteristics of 4G (800 MHz) signals in a typical cellular wireless setup behave very simply as the two-ray-plane Earth model, with approximately 40 dB/decade of signal loss, for almost the entire cell, in contrast to the more common case of finite height receivers with more complex path loss scaling with distance from the transmitter to the receiver. The simple reason behind this is that the "breakpoint" distance, beyond which all models predict this power law, vanishes as the height of the receive antenna vanishes, leading to the unified theory of signal propagation for ground-level receivers in the microwave regime.**

***Index Terms*— 4G, autonomous vehicle.**

I. Introduction

HOW does a microwave propagate between a transmitter and receiver when the receive antenna is at the surface of an imperfect ground plane, such as the Earth? Why would one care about this relatively unexplored regime of wireless propagation? Previous work in the literature on cellular networks operating at microwave frequencies has focused, understandably, on the *horizontal* distance dependence of the path loss between a transmitting and receiving antenna. This is because, by and large, most use cases in 4G/LTE cellular networks consist of a user a few wavelengths to at most a few tens of wavelengths above the ground. The *vertical* distance dependence has not been explicitly considered or systematically measured in the literature for receivers near ground level, i.e., in the limit, the ratio of the receiver height h_{RX} to the wavelength λ goes to zero: $h_{RX}/\lambda \to 0$.

The propagation between antennas in the GHz-range microwave band was extensively studied empirically by Okumura [1] in 1968 and modeled in 1980 by Hata [2], who found an empirical set of equations where the path loss depends on the distance from the transmitter to the receiver as A + B Log10(R). A and B depend on the transmit antenna height (from 30 to 200 m), receive antenna height (1–10 m), and R can be 1–20 km, for a frequency range of 0.15–1.5 GHz. This work is entirely empirical. Although the field has been revisited and refined many times over the last 50 years [3]–[6], the basic empirical conclusions held. Although that empirical work is now literally the industry standard (with models such as the SUI model, the Okumura Model, the Cost-231 Hata model, the Cost-231 Walfisch-Ikegami model, and the Ericsson 9999 model), most use cases to date considered assume (implicitly) that the receiver is a few wavelengths above the ground.

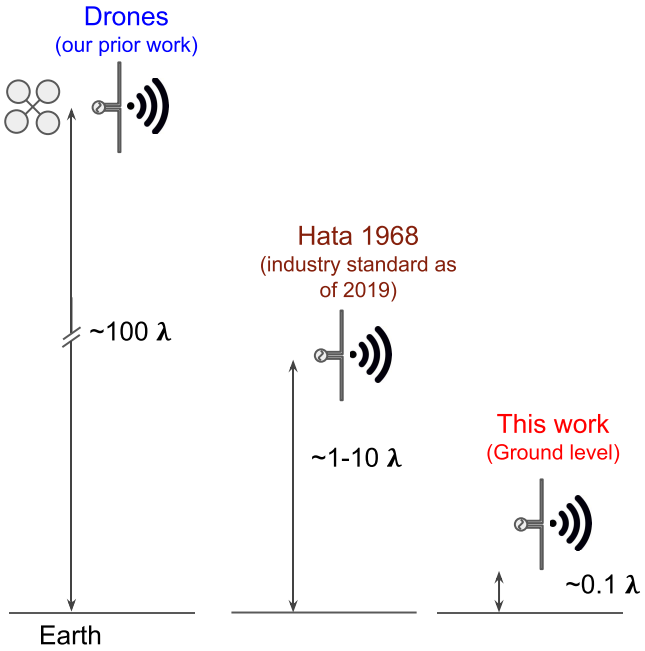

Fig. 1. Schematic comparison of this work versus other work.

The *vertical* dependence of the path loss of actually deployed 4G/LTE systems was recently studied using drone technology [7]–[9] for distances from the Earth from a few to 100 wavelengths. In this work, the complete opposite limit is studied: that of receivers much less than a wavelength above the Earth, which is electrically effectively at the ground level (see Fig. 1). Just like Okumura's data led to 50 years of research and development in wireless propagation where the receiver was a few wavelengths above the ground, this work is expected to provide the first important dataset of receivers at the ground level. A summary of available propagation models is provided and shows that these data are explained by all of them, which predicts a universal scaling law of 40 dB/decade at a distance from the transmitter beyond a "breakpoint" that vanishes in the limit $h_{RX}/\lambda \to 0$.

II. Background, Theory, and Prior Art

For the interpretation of this work, the prior literature on experiments and existing propagation models is discussed in

Manuscript received September 17, 2020; revised June 25, 2021; accepted September 27, 2021. Date of publication January 11, 2022; date of current version April 7, 2022.

The author is with the Department of Electrical and Engineering and Computer Science, University of California at Irvine, Irvine, CA 92697 USA (e-mail: pburke@uci.edu).

Color versions of one or more figures in this article are available at https://doi.org/10.1109/TAP.2021.3137221.

Digital Object Identifier 10.1109/TAP.2021.3137221

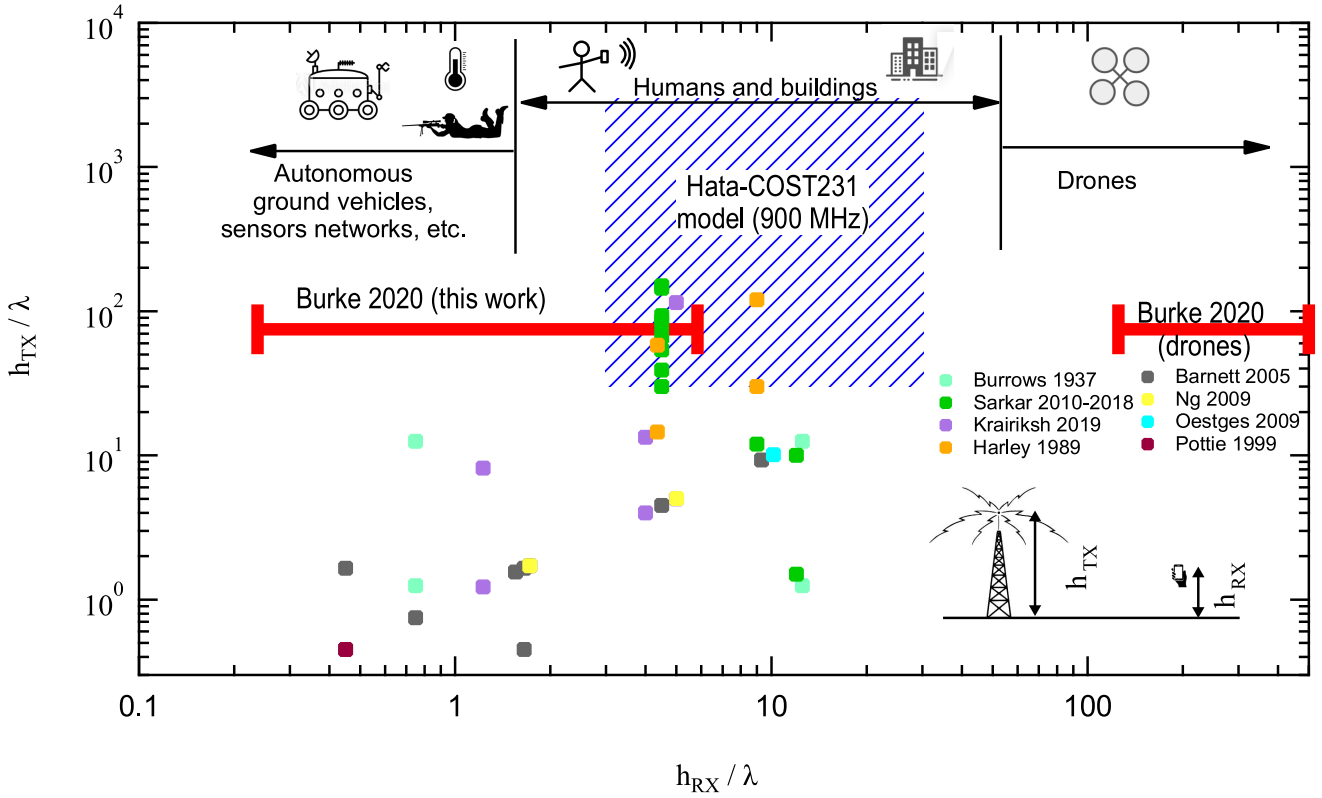

Fig. 2. Various ranges of h_{TX}/λ and h_{RX}/λ used for propagation measurements. The Hata-COST231 model range of the validity is given in the blue hash region for 900 MHz. It is larger if other frequencies are used, but it is not intended for the case $h_{RX}/\lambda < 1$. The data for $hRX/\lambda < 1$ are over water, in dense forest, or indoors. This work, represented by the red line, is the first urban/suburban data in the limit $hRX/\lambda < 1$. Legend: Burrows 1937 [10], Sarkar 2010–2018 [11], [12], Krairiksh 2019 [13], Harley 1989 [14], Joshi 2005 [15], Ng 2009 [16], Oestges 2009 [17], Pottie 1999 [18], and Burke 2020 [7].

this section. By necessity, this will lead to some oversimplifications of a very complex topic, so enough background is provided to put this new experimental data into the appropriate perspective, and this perspective is then being used to explain the contribution of this article to the field.

A. Prior Experimental Work

Reviewing all measurement campaigns is beyond the scope of this article. Rather, salient relevant measurement campaigns that are close to the ground and that deal with the receive antenna height are reviewed. In principle, RX versus TX is symmetric of course according to Maxwell's equations.

In Fig. 2, a summary of available data from the literature for the various ranges of h_{TX}/λ and h_{RX}/λ used for propagation measurements is provided (where h_{TX} is the transmitter height). The published results where $h_{RX}/\lambda < 1$ are for ocean conditions (Burrows 1937 [10]), in dense forests [15], and where the transmitter and receiver are within line of sight (LOS) [18]. Until this article, there have been no published experiments in the microwave range for km-scale distances in dense urban environments at the ground level.

The UCLA work [18] was at 900 MHz, LOS, e.g., within a hallway of an apartment or inside a parking garage. Distances up to 25 m were studied [19]. The decay index n was reported although distance dependence was not presented. The UCLA work also did not study the case of $h_{TX} \gg \lambda$, which is typical in deployed 4G systems.

Joshi *et al.* [15] studied propagation at the ground level in dense forest and LOS on an athletic field. Joshi [15] focused mainly on the loss due to wet, dense foliage. Height dependence in LOS was measured at distances up to 75 m. In addition, Joshi [15] did not include a high TX antenna as is done here, which is more typical of 4G/LTE "in the field" installations.

In sum, existing experimental data in the literature at low h_{RX} have been reported for distances less than 100 m from TX to RX, typically where there is a direct LOS from transmitter to receiver, and typically has low h_{TX}. There is nothing in the prior literature about the more common case of high h_{TX} low h_{RX}, at km distances, in dense urban environments, typical of the modern scenario of a commercial service provider and a client. This article fills this gap in experimental data.

B. Existing Propagation Models

This article is not a comprehensive summary of all propagation models, so this review is not meant to be complete [20]. From a first principles point of view, geometric optics and geometrical theory of diffraction have been extensively used to explain and develop models for radio propagation characterization. For more in-depth reviews and discussions, the reader is referred to the literature, e.g., [21] and [22]. In the following, the discussion focuses on salient features of existing models that apply to this article, which is focused primarily on experimental work.

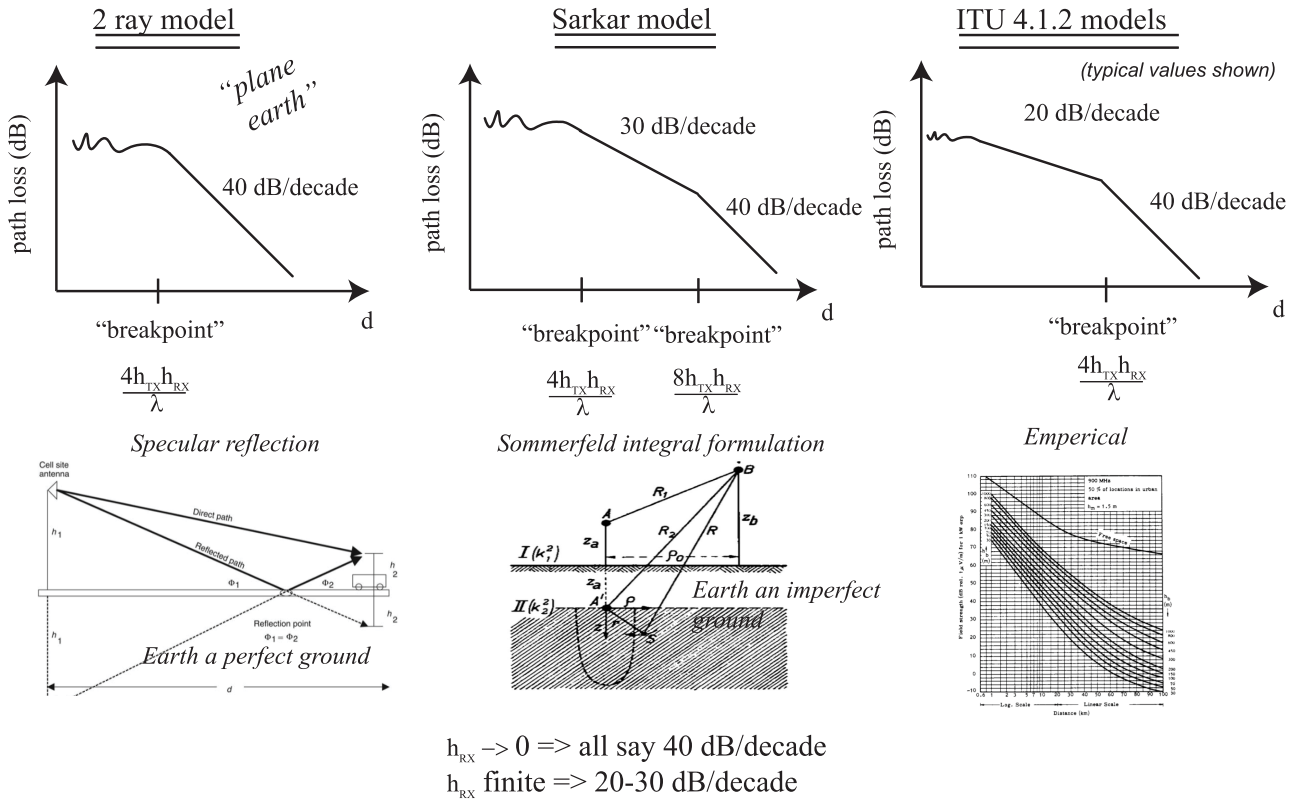

Fig. 3. Summary of various propagation models. The two-ray model assumes that Earth is a perfect conductor. The Sarkar model [21], [23], [24] treats the Earth as an imperfect conductor and provide a rigorous, analytical, physics-based, and intuitive solution based on a formulation pioneered by Sommerfeld over 100 years ago. The ITU model is entirely empirical, based on original work by Hata [2], and new codified in the ITU recommendations [20]. The exact slopes and breakpoints in the ITU models are not universal and vary depending on the environment; only typical predictions are shown for the ITU models. Upper diagrams by the author, and lower diagrams adapted from [2], [21], and [25].

The situation of interest here is where the distance between the transmitter and the receiver is much larger than the height of both antennas. Fig. 3 summarizes the three most commonly used models to describe this case. The first model (two rays or "plane Earth") treats the Earth as a perfect conductor and predicts a path loss power law of -4, i.e., 40 dB/decade, past a breakpoint given by $4h_{TX}h_{RX}/\lambda$. In [25], this is given a clear physical meaning. The two-ray model is a good starting point but misses key features of propagation, such as scattering/diffraction off of buildings and trees, and the imperfect conductivity of the Earth. The next class of models (which we call the Sarkar model) treats the Earth as an imperfect conductor and builds on work by Sommerfeld to create a clear prediction for the path loss beyond two breakpoints: the first being -30 dB/decade and the second -40 dB/decade [21], [23], [24]. Sarkar *et al.* [26] also showed this is a Zenneck wave, not a surface wave. The breakpoints and theory are also physically based.

The third model (or more precisely set of models, based on Okumura's original measurement campaign in Tokyo in 1968 [1]) needs more discussion. The Okumura-Hata and Hata-COST231 models were developed over time as entirely empirical models. They predict a single exponent in the path loss (no breakpoint). However, they were developed for "macrocells," and the scope of use is limited to distances larger than 1 km from the transmitter. This did not apply to so-called "micro cells" where the distance to the transmitter is between 100 m and 1 km, the case studied in this article. Further measurements [27] indicated that a single exponent model does not fit measurements with good accuracy. Therefore, in the spirit of Hata, an empirical "dual-slope" model was developed. Since, in the limit of no scattering other than off a perfect ground plane (the "plane Earth" model discussed above), the dual model is clearly predicted, this empirical dual-slope model in the presence of strong scattering (such as off buildings, terrain, and foliage) had some basis in physical reality, albeit indirect.

For the regime where the distance to the transmitter is between 100 m and 1 km, the ITU has codified all of the existing empirical and semianalytical models into a comprehensive set of predictions in a 50-page document [20]. This includes LOS and non-LOS, and various environments. Although the details depend on the specific environments, a common (although not universal) feature is a change in the path loss exponent at some point in the cell, i.e., the "dual-slope" model, and generally, it varies from 2 to 4, similar to the plane Earth model. However, the ITU model is actually a suite of models for various specific environments. Furthermore, the "breakpoint" of the dual-slope model is not universal in the ITU models. Because, until this article, there was little to no experimental data to base the model on in this limit, the ITU model does not make predictions of the case discussed here,

in the limit $h_{RX}/\lambda \rightarrow 0$. For the LOS case, the breakpoint predicted by the ITU model is given by $4h_{TX}h_{RX}/\lambda$.

In summary, although there are many variations, a common theme is a change in path loss scaling with distance to the transmitter of 40 dB/decade for distances from the transmitter larger than a "breakpoint" given by $4h_{TX}h_{RX}/\lambda$, for all of the existing models in the literature.

C. Contribution of This Article

The primary purpose of this article is: 1) to demonstrate experimentally that the propagation characteristics of 4G (800 MHz) signals in a typical cellular wireless setup at the ground level behave very simply as the two-ray plane Earth model, with approximately 40 dB/decade of signal loss, for most of the cell (which is not the typical situation); 2) to provide an interpretation of this finding based on physics-based literature and empirical-based industry-standard models that are consistent with all three models described above; and 3) to investigate the effect of finite height on these conclusions, experimentally and via interpretation.

What is new about this article in this context is that, usually, the breakpoints appear in the middle or to the edge of a typical cell in a cellular network since $4h_{TX}h_{RX}/\lambda$ is usually 500–1000 m, depending on the TX height, leading to a very complex scaling law within each cell. In contrast, in this work, the predicted breakpoint occurs very close to the transmitter, e.g., at around 10 m for the ground-level path loss. This measurement campaign is the first to measure propagation in this case, i.e., the case where the breakpoint is predicted to be very close to the transmitter (i.e., 10 m) compared to the typical cell size of 1 km. Why one would be interested in this unexplored region of antennas and propagation "phase space," i.e., propagation close to the ground is discussed in Section III.

III. Possible Applications of 4G at Ground Level

There are many possible applications of 4G at the ground level, as discussed in the following.

A. Military

Possible military applications include soldiers close to the ground, e.g., in trenches, foxholes, and prone positions, such as snipers. This actually explains an observation by the U.S. Military (USAF, Navy) over 20 years ago [28], [29], which showed for narrowband controlled experiments and commercial PCS experiments with soldiers at the ground level in the prone or laying position convert to standing position: "when the soldier raises his head, the signal goes up by over 10 dB."

B. Environmental Monitoring: From Smart Dust to Nanoradios

For environmental monitoring, an array of sensor networks is typically deployed at or near ground level. "Smart dust" [30] is one example of this, where environmental monitors are a few mm in size and, therefore, in many use cases, only a few mm above the ground. Longer term, even smaller microradios [31]–[35] are even nanoradios [36]–[41], which may be use cases for the work described in this article, since they all could be deployed in the limit $h_{RX}/\lambda \rightarrow 0$.

Fig. 4. Autonomous delivery vehicles: delivery robot being tested in Irvine, CA, USA. Similar trials are underway by Amazon, Kiwi Bot, Starship, and several other startups.

C. Autonomous Ground Vehicles

Autonomous ground vehicles can have many applications, e.g., first responder applications entering hazardous areas, or even delivery applications. Two recent examples from 2019 are shown in Fig. 4. The market for contactless, autonomous delivery has grown during the COVID-19 pandemic. Thus, the applications of this article have become literally worldwide.

IV. Method

A. Platform Technology

A ground-based microrover technology with onboard GPS was used. Details are described in [42]. Briefly, an onboard GPS receiver with of order 1 m position accuracy in XYZ was used as the vehicle drove slowly (under 1 m/h) along a pedestrian sidewalk and path in a residential neighborhood. The received signal strength indicator (RSSI) was simultaneously recorded so that a map of the RSSI versus position could be obtained. The GPS data were verified to be good at all times by looking at the HDOP and confirming it below 1. HDOP is an indicator of GPS signal quality.

The software for the RSSI mapping runs on a Linux single-board computer onboard the vehicle. The 4G modem is interfaced with the Linux computer through a USB interface. The software for the mapping is open source and has been provided as a service to the research community by depositing on a Git repository at https://gitlab.com/pjbca/4guav/tree/master/getRSSIbuild.

B. Receiver

The RX system was a USB-connected 4G/LTE Novatel/Verizon modem (Model USB 730 L) with an external antenna port.

1) RSSI: The Novatel/Verizon firmware gives the channel and RSSI (in dBm) via a software interface to the device. This article assumes that a large manufacturer would provide an accurate RSSI and validate it with spectrum analyzer measurements; otherwise, the FCC would not have approved it for mass commercial manufacture and use on the consumer 4G network. For the purposes of this article, the relative path loss versus position is what is measured, so the absolute calibration of the RSSI is not critical.

Although the academic community would like to know the details of every single measurement device, the use of a commercial receiver with proprietary circuits is an accepted standard. For example, it has been trusted in [11], where RSSI indications of a commercial cell phone (Nokia 6150) are trusted as accurate and correct without extensive author-based spectrum analyzer measurements and calibrations of power levels. In this article, the same approach is taken, which is to trust the manufacturers' RSSI indicator. If the absolute calibration is off, it does not affect the measurements in this article, as only the relative path loss is what is focused on (below).

The 3GPP standard has set a requirement [43] for LTE receiver absolute power accuracy of ±6 dB under normal conditions and relative accuracy of ±2 dB under normal conditions (which is called RSRP in LTE), and this receiver is LTE certified, so that at least it can be expected to perform that well, if not better.

2) Measurement Time: The RSSI is provided with an update rate of about one sample per second. With a max speed of 1 m/h, this means that the largest error in position for a given RSSI value is about 0.5 m, which is comparable to the GPS accuracy.

3) Sensitivity and Dynamic Range of the Receiver: The minimum connectable power was −120 dBm although typically anything less than −110 dBm led to disconnect from the network. The maximum measured power was −70 dBm. Signals as large as −40 dBm can be detected; therefore, the dynamic range was larger than 80 dB for this measurement campaign, which is sufficient, as the data show.

4) Frequency: The logging software (see GitLab link above) continuously monitored the channel the modem was operating on through its interface. Since the channel is allocated to a specific range of frequencies by the FCC, the frequency range can be logged. In this measurement campaign, the logged channel was 13 for the entire project, which is 750–800 MHz (777–787 MHz uplink and 746–756 MHz downlink). Thus, one is sure about the transmitted and received frequency in this measurement.

C. RX Antennas

The modem was mounted on the back of the rover vehicle, and the antenna connector (TS9) was located approximately 4 in above the ground level, which is roughly a quarter of a wavelength at the frequencies used. A picture of the antennas is shown in Fig. 5. Three antennas were used for this work: A whip antenna as purchased, a modified whip antenna (discussed below), and a resonant dipole antenna. We describe each in the following.

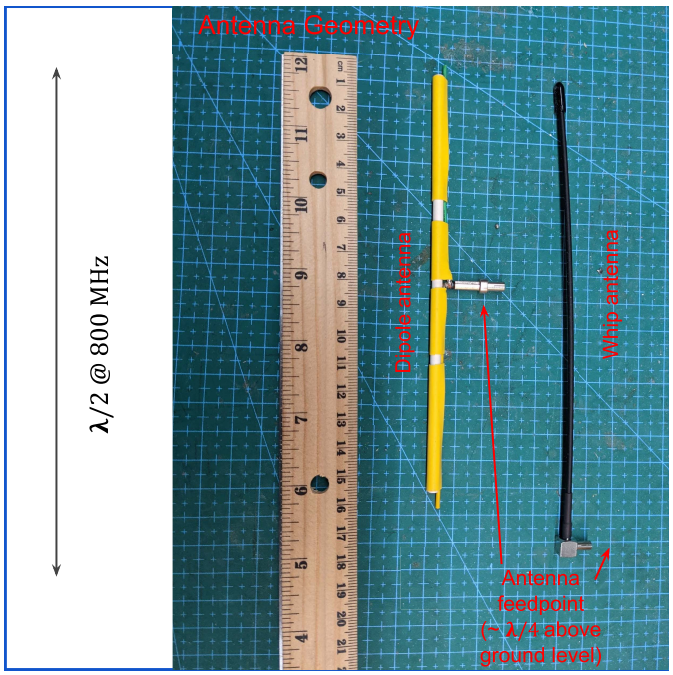

Fig. 5. Antennas used for this work.

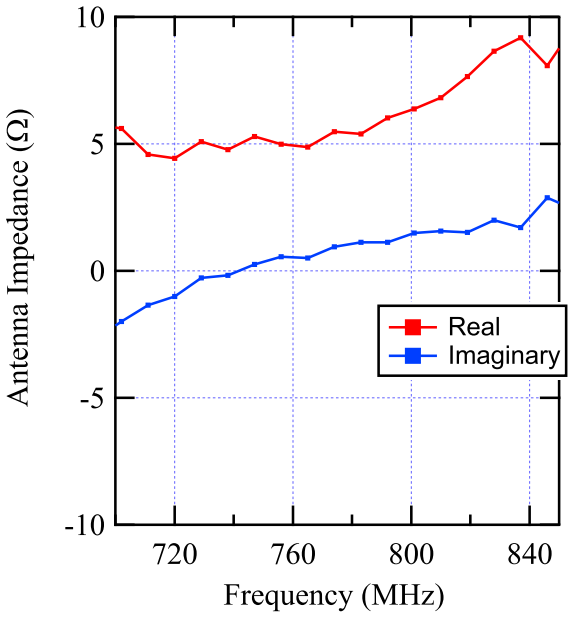

Fig. 6. Antenna impedance for the whip antenna (stock length).

The main characteristics of the antennas of concern here are given as follows:

1) azimuthally symmetric radiation pattern;
2) vertical polarization.

D. RX Antenna 1: Whip Antenna

1) Model Number: A model number Eightwood 4A2-0128-T04RA-050 × 10 external whip antenna with 2 dBi gain was used with a TS9 connector to the receiver. According to the manufacturer, the antenna is meant to cover all the 4G bands, i.e., 791–821, 832–862, 1710–1785, 1805–1880, 2500–2570,

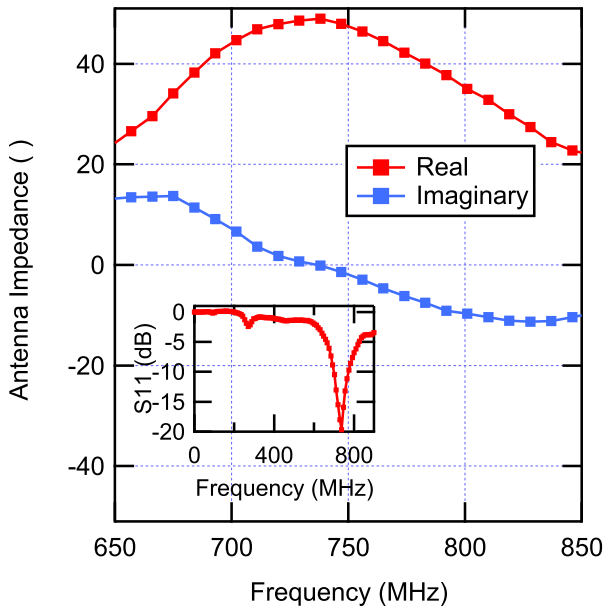

Fig. 7. Antenna impedance for the dipole antenna.

Fig. 8. Drone photograph of the neighborhood showing the transmit tower location. The ground vehicle path was from the bottom to the top of the screen, roughly.

and 2620–2690 MHz, with VSWR $<$ 2.0. This was indeed tested experimentally.

2) Antenna Impedance Characterization: In order to verify the antenna performance in the band used for this measurement, the input impedance of the antenna was characterized using a vector network analyzer (VNA). The results are shown in Fig. 6. Although the antenna is not particularly well-matched, it was sufficiently sensitive for these measurements. It served as a perfectly acceptable antenna to measure the relative path loss versus position.

This antenna was for the first round of propagation measurements. However, the primary resonance occurred well below the advertised band. That is why, in the band of interest, the real impedance is only 5 Ω. Users should beware of advertised antenna performance and verify for themselves.

The whip antenna was modified for the height gain measurements (see below), and its length was adjusted, so the first resonance occurred at around 750 MHz. In that case, the resonance was still weak, and the real impedance was only

Fig. 9. Color scale of RSSI (for the whip antenna at the ground level) overlayed on Google Earth map of the route. The location of the transmit tower is shown at the top of the figure. For the rainbow color scale, red is −65 dBm, and blue is −120 dBm.

Fig. 10. Topographical map showing terrain (from opentopomap.org). The building ET303 is the transmitter location, which is at 15 m above the measurement campaign beginning height above sea level. The measurement campaign covered south of the Peltason drive, which is at 50 m above sea level, all the way to 90 m above sea level at the southernmost point. Since the measurement campaign started at 50 m, an effective height of 15 m (building height of 25–10 m altitude dip from measurement campaign starting point) of the TX is used for this article.

about 10 Ω. The RSSI increased a few dB as expected under identical conditions (i.e., stock whip antenna versus shortened whip antenna).

In summary, both the stock and shortened whip antennas were used for the height gain measurement, but the stock whip

antenna was used for the propagation survey (as well as the dipole, discussed below).

3) Polarization: By symmetry, the antenna geometry makes it sensitive to vertical polarization, similar to a dipole antenna.

4) Azimuthal Symmetry: The antenna was mounted on the side of the vehicle, and it was very close to the ground. The received power might be strongly affected by the driving direction of the vehicle, i.e., the environment changes when the vehicle faces another direction with respect to the transmitter. In order to confirm that this was not a factor, the azimuthal symmetry was measured by rotating the vehicle in place around 360. The relative signal strength did not change by more than 2 dB as a function of azimuthal angle, indicating that the relative orientation of the vehicle was not a major factor in the propagation loss measurement.

5) Sensitivity to Local EM Environment: Experimentally, no significant dependence of the whip antenna impedance on the presence of a concrete ground was found, i.e., the ground did not significantly affect the measured S_{11} as the antenna was raised about the ground.

E. RX Antenna 2: Dipole Antenna

A homemade dipole antenna was used based on 22 gauge solid copper wire and a TS9 connector, supported by an insulating rod with shrink wrap (see Fig. 5). The length was adjusted to be resonant at 750 MHz.

1) Antenna Impedance Characterization: Similar to the whip, the input impedance of the antenna was characterized using a VNA. The results are shown in Fig. 7. The impedance match is excellent in the band of interest.

2) Polarization and Azimuthal Symmetry: By symmetry, the antenna geometry makes it sensitive to vertical polarization. The azimuthal symmetry was measured by rotating the vehicle in place around 360°. Again, the relative signal strength did not change by more than 2 dB as a function of azimuthal angle, indicating that the relative orientation of the vehicle was not a major factor in the propagation loss measurement.

F. Height Gain Methods

The path loss (see below) was measured at the "ground level" with the antenna drive point at 4″ above the ground (approximately a quarter wavelength). For the dipole antenna, the lower arm was, therefore, about 1″ above the ground. For the whip antenna, the arm was positioned above the drive point. The path loss was also measured when the antenna drive point was 2 m above the ground. Both these measurements were done with the dipole and whip antennas on separate runs. Thus, four path loss "maps" were created for each of the permutations of ground level/2 m and whip/dipole antenna. During the 2 m path loss surveys, the vehicle was placed temporarily on the ground for 1 min at several points along to confirm the height gain (i.e., the difference in path loss at the ground level versus 2 m).

In addition, the relative path loss was determined at a fixed point for the dipole, whip (stock length), and whip (shortened) by raising the system one foot at a time above the ground at a fixed location. In addition, the height gain at two different locations was surveyed using the whip (stock length) antenna.

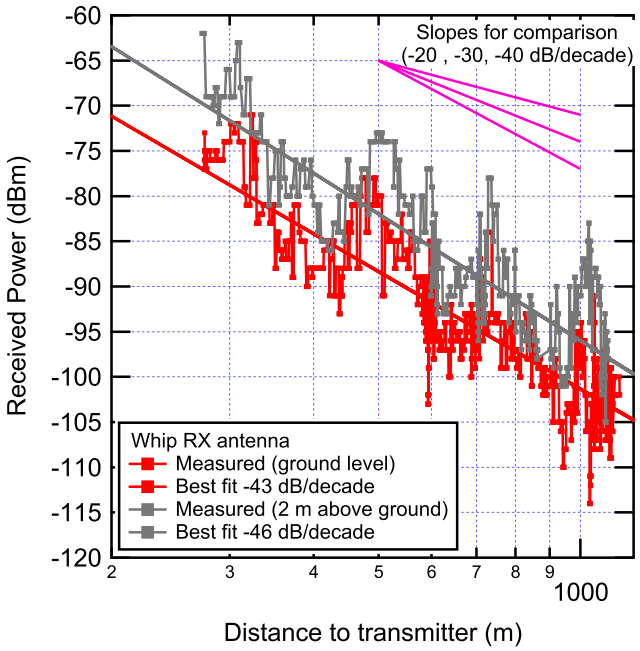

Fig. 11. RSSI versus distance measured along a "proper route" and best power law fit to the data for the whip RX antenna at the ground level and 2 m.

G. Path Loss Determination

In this measurement campaign, the RSSI is used as a measure of the *relative* path loss. (The base station location was known in this case although the TX power is not known.) This gives plenty of information about the physics of the problem, even if the absolute path loss is not measured. It is common in the antenna and propagation literature to fit data to the form [22]

$$PL(dB) = PL(d_0) + 10\ n\ log\left(\frac{d}{d_0}\right) \tag{1}$$

where d_0 is the "reference" position. Since, in this work, the absolute path loss is not measured, it is not possible to determine the reference position d_0. Abdallah *et al.* [12] have argued that d_0 has dubious physical meaning. What is plotted is exactly what Rappaport [22] suggested, which is to find the slope: "when plotted on a log–log scale, the modeled path loss is a straight line with a slope equal to 10n dB per decade. The value of n depends on the specific propagation environment. For example, in free space, n is equal to 2, and when obstructions are present, n will have a larger value." This is precisely the analysis that is carried out in this article.

V. Results

A. Environment

The environment was a residential hilly neighborhood. LOS of the transmitter was intermittent so most of the route was non-LOS. This is accentuated because the receiver was so

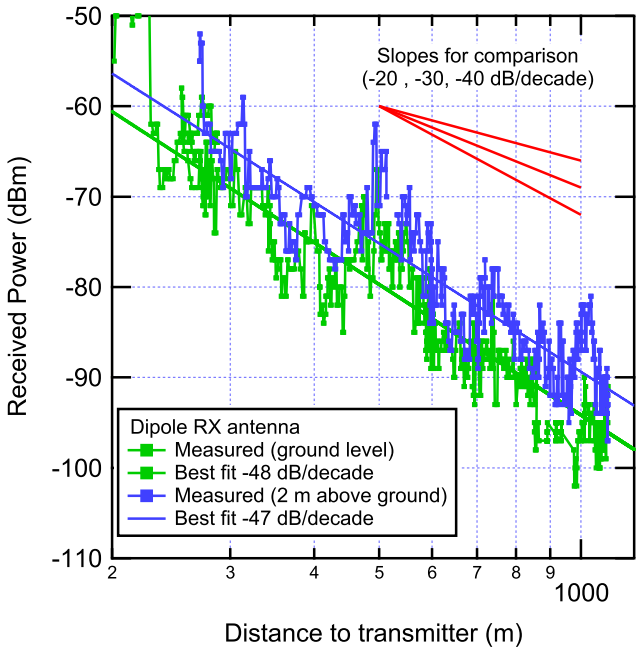

Fig. 12. RSSI versus distance measured along a "proper route" and best power law fit to the data for the dipole RX antenna at the ground level and 2 m.

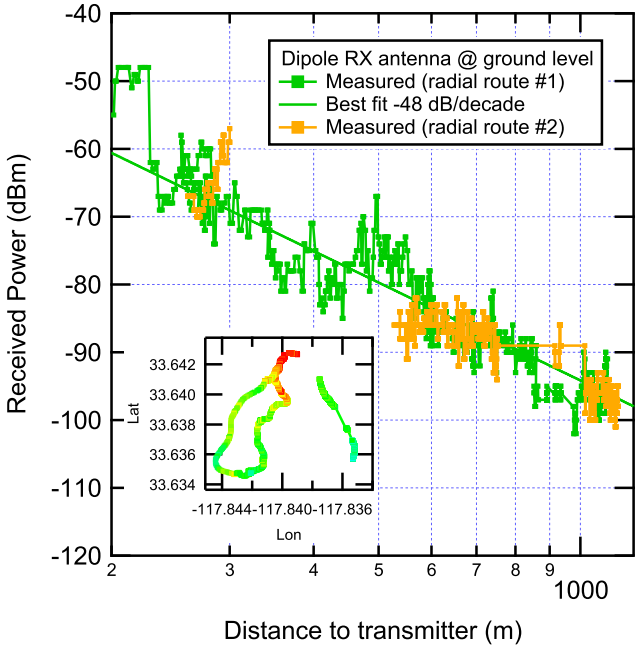

Fig. 13. RSSI versus distance measured along two radials ("proper routes") for the dipole RX antenna at the ground level. Radial 1 was presented in the previous figure (green) in comparison to radial 2 (orange). (Gaps in the orange data due to a disconnected USB connector to the 4G modem during part of the survey.) The inset shows the color-coded RSSI on a lat/lon plot, radial 1 is the proper route discussed above, and radial 2 is the rightmost proper route.

low to the ground. An image of the neighborhood with the cell tower location is shown in Fig. 8 and mapped in Fig. 9. The cell TX antenna is on top of an eight-story building (Engineering Tower, building 303 in Fig. 10) so that the effective transmit antenna height was approximately 15 m above the edge of the survey region. A detailed topographical map shows the height of the terrain in Fig. 10.

B. Path Loss "Map"

A color scale RSSI map overlayed on a Google maps image is shown in Fig. 9 for the whip antenna at the ground level. Most of the terrain is a gently rising hill with the bottom of the image at the highest point.

C. Distance Dependence

The RSSI (in dBm) versus the distance from the base station for the whip antenna at the ground level is shown in Fig. 11 and for the dipole RX antenna in Fig. 12. Also shown are three slopes with arbitrary offsets, for comparison to the data, discussed in Section VI. This section only reports the experimental data; the interpretation and curve fitting is reserved for Section VI.

To test whether the scaling law depends on the radial route chosen, a different radial route was chosen, as shown in Fig. 13, in a similar environment (residential neighborhood with two-story homes.) The figure shows that the scaling law does not depend on the particular radial route chosen, as long as the environment is similar.

D. Environment Dependence

In principle, one should test this scaling law in different environments in the same location. For example, to the

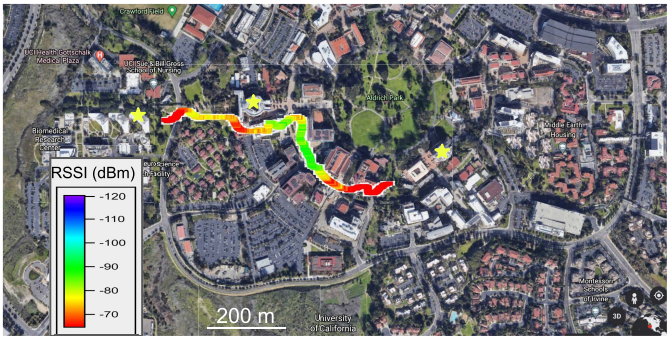

Fig. 14. Color scale of RSSI (for the dipole antenna at the ground level) overlayed on Google Earth map of a route to the east of the base station. The locations of the three transmit towers are shown as gold stars. In the data in previous figures in this article, the rightmost base station is the only one used. However, to the east of this base station, there are many additional base stations. For the rainbow color scale, red is −65 dBm, and blue is −120 dBm. In this densely populated region, in contrast to the residential neighborhood, the towers are closer than 200 m (see scale bar). Therefore, the data of the routes to the south used in this study can be used to measure the propagation, but the routes in the densely populated east cannot be used due to the close proximity of multiple base stations and the fact that the API is proprietary and does not show handoffs from the base station to the base station.

North/West/East of the cell tower are high buildings (ten stories), whereas the routes described above were for the region south of the tower, with only residential (two-story) buildings. Due to the dense population at the university to the north/east/west, there were multiple towers in close vicinity. Since the API is proprietary and does not give the identity of the cell tower, this method could not be used in the region with

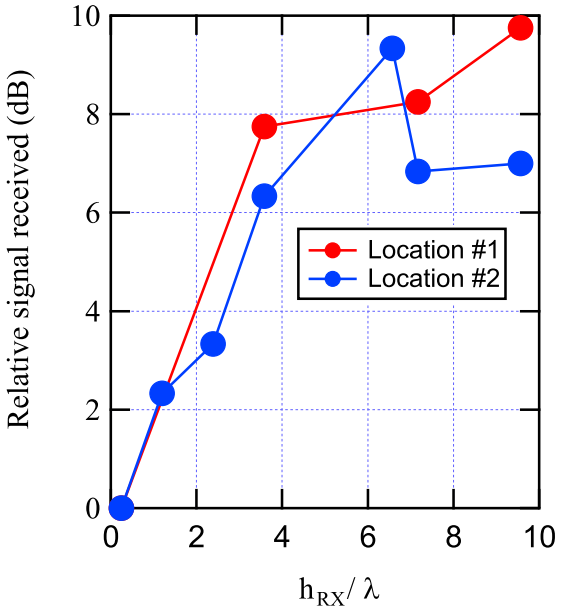

Fig. 15. RSSI versus height of RX antenna at two different locations, both at 1 km from the transmit antenna.

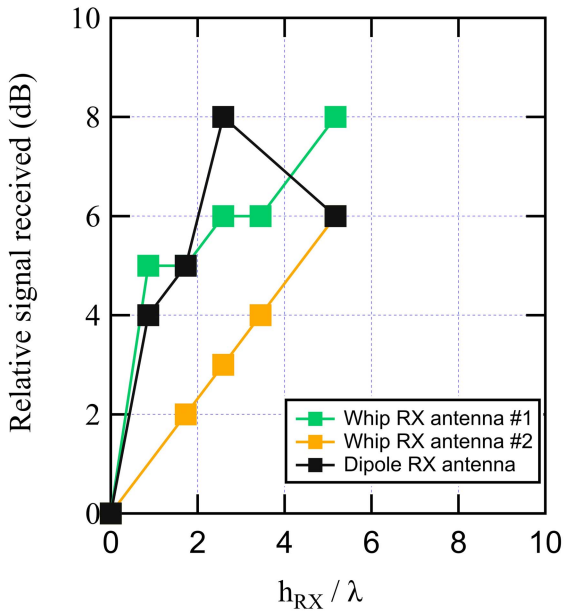

Fig. 16. RSSI versus height of RX antenna at a single location 1 km from the transmit antenna for three different RX antennas (whip stock, whip shortened, and dipole).

close cells. Thus, the southern radial route was the "perfect" location for testing the scaling law all the way out to more the 1 km away from the base station. Fig. 14 shows an RSSI map, which shows that there are three towers within 1 km. The modem is handed off to the nearest (most powerful) base station, indicated by the icons in the figure. Although it is beyond the scope of this work, future research should set up a "test" base station to measure the scaling law in different environments. This work, thus, "paves the way" for many additional studies, just as Hata's original work did in the 1960s.

E. Measurement of Height Dependence

The signal strength was measured as a function of height off the ground from ground level to 2.5 m (approximately 10 λ) in two different locations at a distance of 1 km from the transmitter and also at a fixed location with three different receive antennas. For one of the locations, there were buildings blocking LOS to the base station and very close (within 3 m) to the vehicle. For the other location, it was in an open field, and there was an LOS to the base station. There were no buildings or structures (trees and so on) within 30 m (10 λ) of the vehicle in the second location. In Fig. 15, the signal strength versus height is shown, normalized to the ground level, measured at two locations using the stock whip antenna. In Fig. 16, the signal strength versus height is shown, normalized to the ground level, measured at a single location at 1 km from the transmit antenna using three different antennas: the stock whip antenna, the modified whip antenna, and the dipole antenna. The results are independent of the antenna type used. This is as expected since the radiation patterns of all three antennas are similar. The overall height gain is around 6 dB when raising the antenna from 0.1 λ to 5 λ.

TABLE I
STATISTICAL PROPERTIES OF CURVE FITS

Ant.	$h_{RX}(m)$	r^2	Variance (dB)
Dipole	0.1	0.83	3.5
Dipole	2	0.82	3.8
Whip	0.1	0.80	3.5
Whip	2	0.72	4.5

VI. DISCUSSION AND ANALYSIS

Now that the raw data have been presented, it can be fit and analyzed in this section.

A. Power Law Fitting

In order to fit the power law to the measurement data, this article uses a notion of "proper routes," invented by Abdallah *et al.* [12]. The idea is that, in order to average over large-scale fluctuations in order to find the underlying physics of the power law, one uses a subset of the driving data, which is a radial motion away from the transmitter. In this case, the easternmost path (see Fig. 9) is used, as the driving direction is only radially away from the transmitter.

The rapid fluctuations in the data (fast fading) are due to the multipath/scatterers in the proximity of the receiver. We have plotted these as raw data rather and then filtered them out via smoothing, which is normally done in the literature. In this case, the trend is apparent to the naked eye, so filtering is not needed for the reader. We have verified that the fit of the slope is the same whether the fast fading is filtered or not. The average distance between each point is about 1 m, i.e., a few wavelengths.

1) Path Loss Exponent Calculation: The power loss exponent for the measured data was determined by fitting a line

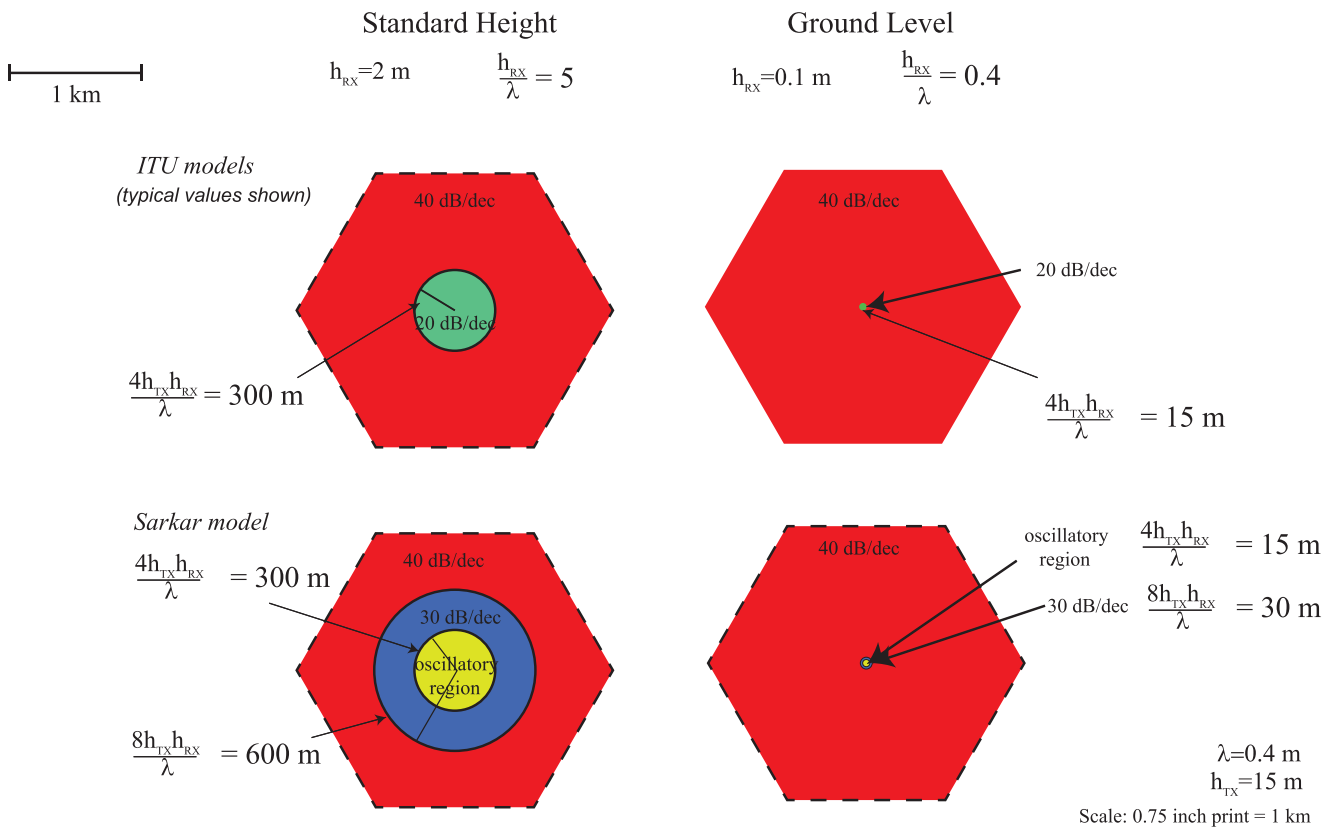

Fig. 17. Typical cell is of order 1 km on a side, shown as a hexagon. Within this cell, various models predict various decay exponents depending on the value of the breakpoints. For normal antenna height (1.5 m), the breakpoints are inside the cell. For ground-level antenna (0.1 m), the breakpoints are very near to the transmitter, and most of the cell is in the 40 dB/decade limit, independent of the particular model used. Parameters assumed are 0.75 GHz, and $h_{TX} = 15$ m. The exact slopes and breakpoints in the ITU models are not universal and vary depending on the environment; only typical predictions are shown for the ITU models. The purple lines show the range of distances for this measurement campaign.

to RSSI versus log d. The results are shown as the solid lines in Figs. 11 and 12, indicating an exponent of between −43 and −48 dB/decade at the ground level and between −46 and −47 dB/decade at 2 m. This is approximately the predicted −40 dB/decade predicted by the two ray and other models, as discussed in the following, for distances far from the transmitter. A geometric interpretation of this is given in the following.

2) Variation: In order to determine the quality of the fitting, the coefficient of determination (usually called simply "r-squared") was determined for each fit. Table I shows the values calculated, which are between 0.7 and 0.8. Statistical variations of the signal around the median value were also calculated, defined as $\sqrt{(\chi^2)/N}$, as commonly considered in the literature. (Here, χ is $RSSI_{measured} - RSSI_{expected}$ and N is the number of points.) The variation around the expected level is around 3–4 dB. These serve to quantify the fit, as shown in Figs. 11 and 12.

It should be noted that this implicitly assumes that the errors are normally distributed with zero mean and constant variance, and the fit function is a good description of the data, i.e., at any value of d, the path loss is random and distributed log-normally about the mean distance-dependent value, so the fluctuations are a Gaussian distributed random variable (in dB). This is what is commonly assumed in the path loss survey literature [22].

B. Geometrical Explanation of Path Loss Exponent

A common feature of all propagation models is that they all converge to the two-ray model prediction of a 40 dB/decade path loss after a "breakpoint," which depends on the heights of the two antennas and the wavelength (see Fig. 3) as $4h_{TX}h_{RX}/\lambda$. (The prediction for the ITU models is not universally 40 dB/decade and depends on the environments but is approximately 40 dB/decade in most cases.) In prior experiments, this "breakpoint" was typically a few hundred meters or more. In this article, the low value of $4h_{TX}h_{RX}/\lambda$ gives a predicted breakpoint of between 15 and 30 m for the ground-level data. Therefore, in all of the measurement range (from 250 to 1100 m), all models predict a path loss decay of 40 dB/decade, which is approximately what is observed for the ground-level data.

In order to more explicitly demonstrate this point, Fig. 17 illustrates the predictions of two of the models (Sarkar and ITU), for the "normal" case of an antenna 2 m above the ground, and the case where the receive antenna is only 0.1 m above the ground. For these parameters, and the transmit antenna height of 15 m, at 0.75 GHz, the breakpoints are shown to scale with a typical cell region of order 1 km on a side. The model clearly shows that the ground-level antenna case would experience 40 dB/decade over almost the entire cell, as is shown here.

C. Path Loss at Ground Level Versus 2 m and Versus RX Antenna

In order to further investigate the effects of the RX antenna and the RX antenna height, the same measurement campaign and path loss analysis was performed at 2 m antenna height and for two different antennas: a whip antenna and a dipole antenna. The results for the path loss with the whip antenna at the ground and 2 m level are shown in Fig. 11, together with the best fit path loss. The results for the path loss with the dipole antenna at ground and 2 m level are shown in Fig. 12, together with the best fit path loss. The power law is between −46 and −47 dB/decade at 2 m. The slopes are not sensitive to the range of data used to fit the curves.

1) RX Antenna Dependence: As expected, the power law is not strongly dependent on the RX antenna used. The dipole antenna and whip antenna give comparable path law slopes. The overall path loss difference at the ground level between the two antennas is completely accounted for by the mismatch that the whip antenna provides to the RX 5 Ω input impedance versus the dipole, which is almost perfectly matched (see Section IV-E1). Based on the antenna characterization of the whip antenna, the mismatch would give about a 7 dB difference in path loss between the two antennas (assuming a 5 Ω real impedance as measured). This is almost exactly the difference in path loss for the whip versus dipole antenna at the ground level and also at the 2 m level.

In summary, the only difference that the antenna has in the path loss measurement is completely explained by the mismatch to the RX input. It seems that the radiation patterns (which are both azimuthally symmetric) have an insignificant or minor effect on the path loss.

2) RX Height Dependence: Slope: The height dependence of the path loss slope is discussed next. The experiments show that the slope is nearly identical in the region studied (250–1200 m from the transmitter). This is in an agreement with the ITU (empirical) models, which predict approximately 40 dB/decade beyond 300 m (this campaign starts at 250 m).

For the Sarkar model, where does the two-ray regime (red region in Fig. 17) begin for the 2 m RX height case? The predicted answer eight times $h_{TX}h_{RX}/\lambda$. The model predicts a 30 dB/decade slope between 300 and 600 m. Although this is not observed clearly, it is very difficult for this particular dataset to determine the mean slope in such a narrow region of the distance between transmitter and receiver. Further possible reasons for not observing the expected −30 dB/decade in the region 300–600 m for the 2 m high RX data include the following.

1) The polarization is not modeled or accounted for in this measurement campaign, which is known to affect the power law in this intermediate region [12], [44].
2) The variation in the data is too large to observe a meaningful slope of 30 versus 40 dB/decade over such a narrow distance range. (The drop in signal would be either 9 or 12 dB over 300–600 m for −30 versus −40 dB/decade slope, which is comparable to the statistical variation in the measurement data; see Table I).

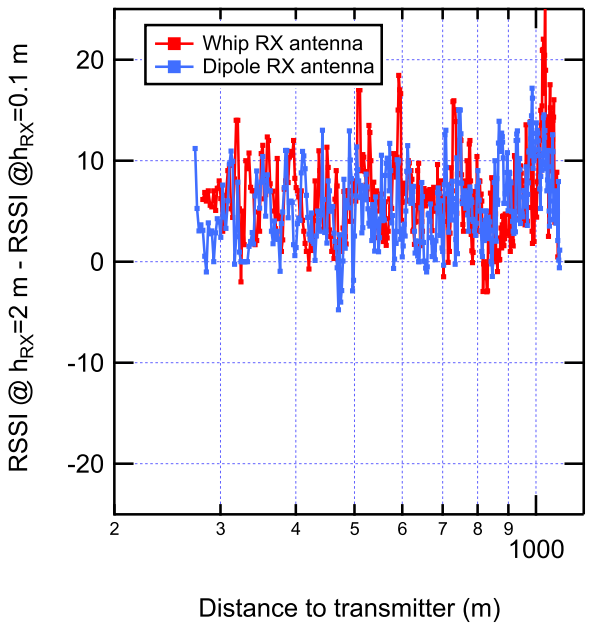

Fig. 18. "Height gain" versus distance for both dipole and whip RX antennas.

3) The "proper route" method employed here provides additional uncertainty in the path loss exponent averaged over all of xy space, which is not accounted for in the statistical analysis. In other words, to get the slope of the mean path loss between 300 and 600 m, accurately measured, it would require much a much more extensive dataset given the statistical fluctuations about the mean. Although that is not possible with current technology, the prospects to develop a technology to achieve this are discussed in more detail in the following.

D. RX Height Dependence Versus Distance From TX: Expected Behavior

Although the extrapolation to zero height was not explicitly considered in prior models, they all have some height-dependent expectations that can be extrapolated to zero. The two-ray model predicts that the received power is simply given by $P_r/P_t = G_{TX}G_{RX}(h_{TX}h_{RX}/d^2)^2$, i.e., a 20 dB/decade change in signal with respect to h_{RX}. The Hata model has some empirical dependence built in, but it does not apply near ground level. The Sarkar model makes similar predictions to the two-ray model (discussed extensively in [44]) although it is a more rigorous model and includes more numerical results.

E. RX Height Dependence Versus Distance From TX: Observed Behavior

Consistent with the model expectations for finite height receivers, the path loss versus height (see Figs. 15 and 16) both showed that the path loss decreases as the antenna height increases. In addition, the "height gain" from 0.1 to 2 m (defined as the path loss difference) is plotted in Fig. 18 versus the distance from the transmitter for the whip and dipole RX

antenna. Both sets of data show fluctuations of order ±5 dB about the mean of 5 dB height gain, independent of distance up until around 1 km from the transmitter, where this is a slight upturn. This is consistent with all three models that predict some height gain, regardless of distance from transmitter or RX antenna used.

VII. Perspectives for Future Work: Scaling and Drone Technology

In order to enable a larger dataset to better determine the mean path loss versus distance to the transmitter, one would like to measure the path loss in more than a line. Ideally, one would like to measure the path loss on a 2-D grid of points spaced by of order λ (e.g., 0.4 m or 15″) at a height of 0.1 λ (0.04 m or 1.5″) over a 2-D plane of 1 km × 1 km. How would one do this?

To do this, one would need a microrover that was capable of navigating rocks and rocky terrain, steps, street bumpers, tall and short grass, bushes, trees, and even the inside of buildings, over a 1 km square, populated area, while still keeping the antenna at a few inches above the ground. Other than the privacy and permission issues, the microrover technology just does not exist yet to perform this at scale. The rover used in this work was confined to smooth terrains, such as sidewalks and smooth dirt paths.

For such a scheme, drone technology [7]–[9] at low altitude (i.e., at 1.5″ of altitude) would be a more appropriate and a possible technological solution to the measurement challenge. Such a survey is even slightly beyond the capability of existing drones but could feasibly be developed with additional effort. Privacy and easement issues in a dense urban environment of course would have to be addressed at this scale. These exciting technological challenges and opportunities, developments of which are currently underway in the author's labs, are beyond the scope of this article and remain for future research.

VIII. Conclusion

In conclusion, this article presented experimental data from a measurement campaign of "in the wild" 4G/LTE signal propagation for an antenna at the ground level. This provides the first (albeit small) set of data in this new, relatively unexplored regime, and the first comparison (experimental) of ground level versus normal, from $h_{RX}/\lambda < 1$ to $h_{RX}/\lambda > 1$. A summary of available propagation models showed that the data are explained by all of them since the ground limit of the receiver forces the "breakpoint" for the different power laws to be close (within 50 m) to the transmitter, explaining the experimental finding of approximately 40 dB/decade in the limit $h_{RX}/\lambda \to 0$.

References

[1] Y. Okumura, E. Ohmori, T. Kawano, and K. Fukuda, "Field strength and its variability in VHF and UHF land-mobile radio service," *Rev. Elect. Commun. Lab.*, vol. 16, nos. 9–10, pp. 825–873, 1968.

[2] M. Hata, "Empirical formula for propagation loss in land mobile radio services," *IEEE Trans. Veh. Technol.*, vol. VT-29, no. 3, pp. 317–325, Aug. 1980.

[3] M. F. Iskander and Z. Yun, "Propagation prediction models for wireless communication systems," *IEEE Trans. Microw. Theory Techn.*, vol. 50, no. 3, pp. 662–673, Mar. 2002.

[4] S. A. Mawjoud, "Comparison of propagation model accuracy for long term evolution (LTE) cellular network," *Int. J. Comput. Appl.*, vol. 79, no. 11, pp. 41–45, Oct. 2013.

[5] A. I. Sulyman, A. T. Nassar, M. K. Samimi, G. R. MacCartney, Jr., T. S. Rappaport, and A. Alsanie, "Radio propagation path loss models for 5G cellular networks in the 28 GHz and 38 GHz millimeter-wave bands," *IEEE Commun. Mag.*, vol. 52, no. 9, pp. 78–86, Sep. 2014.

[6] M. Mollel and M. Kisangiri, "Comparison of empirical propagation path loss models for mobile communication," *Comput. Eng. Intell. Syst.*, vol. 5, no. 9, pp. 1–11, 2014. [Online]. Available: http://iiste.org/Journals/index.php/CEIS/article/view/15435

[7] P. J. Burke, "Demonstration and application of diffusive and ballistic wave propagation for drone-to-ground and drone-to-drone wireless communications," *Sci. Rep.*, vol. 10, no. 1, pp. 1–12, Dec. 2020, doi: 10.1038/s41598-020-71733-0.

[8] Qualcomm. (2017). *LTE Unmanned Aircraft Systems: Trial Report*. [Online]. Available: https://www.qualcomm.com/documents/lte-unmanned-aircraft-systems-trial-report

[9] M. Nekrasov *et al.*, "Evaluating LTE coverage and quality from an unmanned aircraft system," in *Proc. IEEE 16th Int. Conf. Mobile Ad Hoc Smart Syst.*, Nov. 2019, pp. 171–179.

[10] C. R. Burrows, "The surface wave in radio propagation over plane earth," *Proc. Inst. Radio Eng.*, vol. 25, no. 2, pp. 219–229, Feb. 1937.

[11] T. K. Sarkar *et al.*, "Electromagnetic macro modeling of propagation in mobile wireless communication: Theory and experiment," *IEEE Antennas Propag. Mag.*, vol. 54, no. 6, pp. 17–43, Dec. 2012.

[12] M. N. Abdallah *et al.*, "Further validation of an electromagnetic macro model for analysis of propagation path loss in cellular networks using measured driving-test data," *IEEE Antennas Propag. Mag.*, vol. 56, no. 4, pp. 108–129, Aug. 2014.

[13] M. Krairiksh *et al.*, "Measurement of radiated field from transmitting antennas located in various environments," *IEEE Trans. Antennas Propag.*, vol. 67, no. 4, pp. 2056–2062, Apr. 2019.

[14] P. Harley, "Short distance attenuation measurements at 900 MHz and 1.8 GHz using low antenna heights for microcells," *IEEE J. Sel. Areas Commun.*, vol. 7, no. 1, pp. 5–11, Jan. 1989.

[15] G. G. Joshi *et al.*, "Near-ground channel measurements over line-of-sight and forested paths," *IEE Proc.-Microw., Antennas Propag.*, vol. 152, no. 6, pp. 589–596, Dec. 2005.

[16] Y. S. Meng, Y. H. Lee, and B. C. Ng, "Empirical near ground path loss modeling in a forest at VHF and UHF bands," *IEEE Trans. Antennas Propag.*, vol. 57, no. 5, pp. 1461–1468, May 2009.

[17] C. Oestges, B. M. Villacieros, and D. Vanhoenacker-Janvier, "Radio channel characterization for moderate antenna heights in forest areas," *IEEE Trans. Veh. Technol.*, vol. 58, no. 8, pp. 4031–4035, Oct. 2009.

[18] K. Sohrabi, B. Manriquez, and G. J. Pottie, "Near ground wideband channel measurement in 800–1000 MHz," in *Proc. IEEE VTS 50th Veh. Technol. Conf.*, 1999, vol. 1, no. 3, pp. 571–575.

[19] H. Zaghloul, G. Morrison, D. Tholl, M. G. Fry, and M. Fattouche, "Measurement of the frequency response of the indoor channel," in *Proc. 33rd Midwest Symp. Circuits Syst.*, 1999, pp. 405–407.

[20] *Propagation Data and Prediction Methods for the Planning of Short-Range Outdoor Radiocommunication Systems and Radio Local Area Networks in the Frequency Range 300 MHz to 100 GHz P Series Radiowave Propagation*, Int. Telecommun. Union, Geneva, Switzerland, 2019. [Online]. Available: https://www.itu.int/rec/R-REC-P.1411-10-201908-I/en

[21] T. K. Sarkar, H. Chen, M. Salazar-Palma, and M. D. Zhu, "Physics-based modeling of experimental data encountered in cellular wireless communication," *IEEE Trans. Antennas Propag.*, vol. 66, no. 12, pp. 6673–6682, Dec. 2018.

[22] T. S. Rappaport, *Wireless Communications: Principles and Practice*, vol. 2. Upper Saddle River, NJ, USA: Prentice-Hall, 2002.

[23] T. K. Sarkar, M. N. Abdallah, and M. Salazar-Palma, "Survey of available experimental data of radio wave propagation for wireless transmission," *IEEE Trans. Antennas Propag.*, vol. 66, no. 12, pp. 6662–6672, Dec. 2018.

[24] T. K. Sarkar, H. Chen, M. Salazar-Palma, and M. Zhu, "Lessons learned using a physics-based macromodel for analysis of radio wave propagation in wireless transmission," *IEEE Trans. Antennas Propag.*, vol. 67, no. 4, pp. 2150–2157, Apr. 2019.

[25] J. D. Parsons, *The Mobile Radio Propagation Channel*. Hoboken, NJ, USA: Wiley, 2000.

[26] T. K. Sarkar *et al.*, "Physics of propagation in a cellular wireless communication environment," *URSI Radio Sci. Bull.*, vol. 85, no. 4, pp. 5–21, 2012.
[27] S. R. Saunders, "Advances in mobile propagation prediction methods," in *Mobile Antenna Systems Handbook*. U.K.: Wiley, 2001, pp. 55–140.
[28] R. A. Foran, T. B. Welch, and M. J. Walker, "Very near ground radio frequency propagation measurements and analysis for military applications," in *Proc. IEEE Mil. Commun. Conf. (MILCOM)*, Oct. 1999, pp. 336–340.
[29] T. B. Welch *et al.*, "Very near ground RF propagation measurements for wireless systems," in *Proc. VTC-Spring, IEEE 51st Veh. Technol. Conf.*, May 2000, pp. 2556–2558.
[30] B. Warneke, M. Last, B. Liebowitz, and K. S. J. Pister, "Smart dust: Communicating with a cubic-millimeter computer," *Computer*, vol. 34, no. 1, pp. 44–51, Jan. 2001.
[31] R. Gómez-Martínez *et al.*, "Intracellular silicon chips in living cells," *Small*, vol. 6, no. 4, pp. 499–502, Feb. 2010.
[32] M. Tabesh, M. Rangwala, A. M. Niknejad, and A. Arbabian, "A power-harvesting pad-less mm-sized 24/60 GHz passive radio with on-chip antennas," in *Symp. VLSI Circuits Dig. Tech. Papers*, 2014, pp. 1–2.
[33] L. Y. Chen *et al.*, "Mass fabrication and delivery of 3D multilayer μtags into living cells," *Sci. Rep.*, vol. 3, no. 1, p. 2295, Dec. 2013.
[34] X. Hu *et al.*, "Micrometer-scale magnetic-resonance-coupled radio-frequency identification and transceivers for wireless sensors in cells," *Phys. Rev. A, Gen. Phys.*, vol. 8, no. 1, Jul. 2017, Art. no. 014031.
[35] J. Choi, E. Aklimi, C. Shi, D. Tsai, H. Krishnaswamy, and K. L. Shepard, "Matching the power, voltage, and size of biological systems: A nW-scale, 0.023-mm^3 pulsed 33-GHz radio transmitter operating from a 5 kT/q-supply voltage," *IEEE Trans. Circuits Syst. I, Reg. Papers*, vol. 62, no. 8, pp. 1950–1958, Aug. 2015.
[36] P. Burke and C. Rutherglen, "Towards a single-chip, implantable RFID system: Is a single-cell radio possible?" *Biomed. Microdevices*, vol. 12, no. 4, pp. 589–596, Aug. 2010. [Online]. Available: http://link.springer.com/10.1007/s10544-008-9266-4
[37] P. J. Burke and C. M. Rutherglen, "*In vivo* RFID chip," U.S. Patent 8 830 037 B2, Sep. 9, 2014.
[38] C. Rutherglen and P. Burke, "Nanoelectromagnetics: Circuit and electromagnetic properties of carbon nanotubes," *Small*, vol. 5, no. 8, pp. 884–906, Apr. 2009, doi: 10.1002/smll.200800527.
[39] P. Burke, S. Li, and Z. Yu, "Quantitative theory of nanowire and nanotube antenna performance," *IEEE Trans. Nanotechnol.*, vol. 5, no. 4, pp. 314–334, Jul. 2006.
[40] C. Rutherglen and P. Burke, "Carbon nanotube radio," *Nano Lett.*, vol. 7, no. 11, pp. 3296–3299, Nov. 2007.
[41] G. W. Hanson, "Fundamental transmitting properties of carbon nanotube antennas," *IEEE Trans. Antennas Propag.*, vol. 53, no. 11, pp. 3426–3435, Nov. 2005.
[42] P. J. Burke, "A 4G-connected micro-rover with infinite range," *IEEE J. Miniaturization Air Space Syst.*, vol. 1, no. 3, pp. 154–162, Dec. 2020.
[43] *Evolved Universal Terrestrial Radio Access (E-UTRA); Requirements for Support of Radio Resource Management*, document TS 36.133, Version 10.3.0, 2011. [Online]. Available: http://www.3gpp.org/ftp/Specs/archive/36series/36.133/36133-a30.zip
[44] A. De, T. K. Sarkar, and M. Salazar-Palma, "Characterization of the far-field environment of antennas located over a ground plane and implications for cellular communication systems," *IEEE Antennas Propag. Mag.*, vol. 52, no. 6, pp. 19–40, Dec. 2010.

Peter J. Burke (Fellow, IEEE) received the Ph.D. degree in physics from Yale University, New Haven, CT, USA, in 1998.

From 1998 to 2001, he was a Sherman Fairchild Postdoctoral Scholar in physics with the California Institute of Technology, Pasadena, CA, USA. Since 2001, he has been a Faculty Member with the Department of Electrical Engineering and Computer Science, University of California at Irvine, Irvine, CA, USA. His current research interests include Electrical Engineering and Computer Science (EECS), Biomedical Engineering (BME), chemical and biomolecular engineering, materials science and engineering, and chemical and materials physics.